Intrinsic Gas-Phase Reactivity toward Methanol of Trinuclear Tungsten W_3S_4 Complexes Bearing W−X (X = Br, OH) Groups

Cristian Vicent,*,† Marta Feliz,‡ and Rosa Llusar*,‡

Serveis Centrals d'Instrumentació Cientifica and Departament de Química Física i Analítica, Universitat Jaume I, Av. Sos Baynat s/n, 12071 Castelló, Spain

Received: May 14, 2008; Revised Manuscript Received: October 17, 2008

Electrospray ionization (ESI) tandem mass spectrometry is used to investigate the gas-phase dissociation of trinuclear sulfide W_3S_4 complexes containing three diphosphane ligands and three terminal bromine atoms, namely, $[W_3S_4(dmpe)_3(Br)_3]^+$ ($\mathbf{1}^+$) or hydroxo groups, $[W_3S_4(dmpe)_3(OH)_3]^+$ ($\mathbf{2}^+$) (dmpe = 1,2-bis(dimethylphosphanyl)ethane). Sequential evaporation of two diphosphane ligands is the sole fragmentation channel for the $\mathbf{1}^+$ cation that yields product ions with one or two unsaturated W−Br functional groups, respectively. Conversely, evaporation of one diphosphane ligand followed by two water molecules is observed for cation $\mathbf{2}^+$. Complementary deuterium-labeling experiments in conjunction with computational studies provide deep insight into the thermodynamically favored product ion structures found along the fragmentation pathways. From these results, the formation of a series of cluster cations with W−Br, W−OH, and W=O functional groups either on saturated or unsaturated metal sites is proposed. The effect of the properties of these cluster cations, among them chemical composition and coordinative saturation, on their reactivity toward methanol is discussed.

1. Introduction

Group 6 oxides play a crucial role in heterogeneous catalysis,[1−4] and current applications include the dehydrogenation and isomerization of alkanes,[5−7] alkene methatesis,[8,9] and the dehydration or oxidation of alcohols to alkenes or aldehydes, respectively.[10,11] The basis for such a wide spectrum of applications relies on the variability of oxidation states, coordination versatility, and rich structural diversity of the group 6 oxides. However, the details of the molecular mechanism of many reactions occurring at the oxide surfaces during the catalytic processes are not yet fully understood in part due to the complexity of the catalyst surface and the possibility of different sites of reaction. Mass spectrometric techniques have recently emerged as a promising approach to obtain fundamental insight into the complicated structures and chemical processes of oxide materials.[12−17] In particular the gas-phase generation of group 6 oxide clusters has been extensively investigated and many efforts have been devoted to divulge the fundamental features of cluster ions with hydroxo M−OH, alkoxo M−OR, and oxo M=O (M = group VI metal) functional groups which are putative active species during the catalytic cycle occurring on the heterogeneous surface.[11,18]

ESI tandem mass spectrometry represents a versatile approach to study the gas-phase ion chemistry of cluster group 6 oxo-complexes. Complementary experimental techniques, such as photoelectron spectroscopy or ion−molecule reactions, in conjunction with computational methods are also employed to obtain deep insight on the electronic and structural characterization of the new gas-phase species generated.[19−25] The formation of gaseous group 6 ions bearing terminal oxo, hydroxo, or alkoxo functional groups is relatively straightforward with ESI.[26−28] For example, the electrospray ionization mass spectra of mononuclear $[MO_4]^{2-}$ (M = Cr, Mo, W) anions in acetonitrile or methanol reveals the presence of terminal hydroxo or alkoxo $[MO_3(OH)]^-$ and $[MO_3(OCH_3)]^-$ anions, respectively.[29,30] However, ESI generation of higher nuclearity complexes with M=O, M−OH, or M−OR groups with well-defined electronic and molecular structures heavily relies on the availability of preexisting polynuclear entities in solution.[31−33] In this sense, the isolation of cluster compounds with terminal hydroxo ligands has remained a challenge mainly due to their strong tendency to form polynuclear oxo-bridging through hydrolysis and subsequent donation of the OH group lone electron pairs to the empty coordination site of a second molecule.[34]

Recently, our group has reported the synthesis of the terminal hydroxo complex formulated as $[W_3S_4(dmpe)_3(OH)_3]^+$ starting from the bromide $[W_3S_4(dmpe)_3(Br)_3]^+$ analogue.[35,36] Each trinuclear W_3S_4 cluster unit contains one hydroxo or bromine terminal ligand coordinated to a tungsten site in an overall C_{3v} symmetry. Schematically, the trinuclear cluster $[W_3S_4(dmpe)_3(X)_3]^+$ (X = Br, OH) complexes are shown in Chart 1a,b.

Each trinuclear unit is composed of three tungsten atoms defining an equilateral triangle, one capping sulfur atom and three bridging-sulfide ligands (Chart 1a). The environment around each tungsten site is filled by one bromine or hydroxo group and one diphosphane ligand, which sterically hinders the W−OH groups preventing its hydrolysis. The incomplete-cuboidal W_3S_4 unit is electron precise with six metal electrons for the formation of three W−W bonds and a formal +4 oxidation state for the W atoms.[37] The gas-phase reactivity investigation of these complexes might be instructive as a way to model the behavior of metal oxide surfaces due to several reasons: (i) they present neighboring terminal hydroxo ligands which might simulate the presence of these groups in the

* Corresponding author.
† Serveis Centrals d'Instrumentació Cientifica. E-mails: barrera@sg.uji.es. Tel: +34 964387344. Fax: +34 964387309.
‡ Departament de Química Física i Analítica. E-mail: feliz@qfa.uji.es (M.F.) and llusar@qfa.uji.es (R.L.). Tel: +34 964728086. Fax: +34 964728066.

10.1021/jp804263q CCC: $40.75
Published on Web 11/14/2008

CHART 1: Representation of Trinuclear $[W_3S_4(dmpe)_3(X)_3]^+$ (X = Br, OH) Complexes[a]

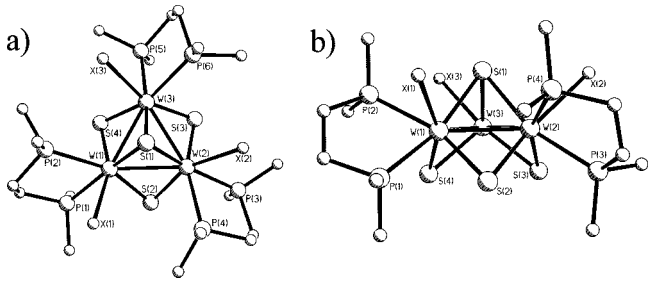

[a] For clarity, one of the diphosphane ligands is omitted in part b.

heterogeneous solids, (ii) they possess well-defined molecular and electronic structures and therefore facilitate product ion structure assignments, and (iii) they additionally bears neutral diphosphane ligands which can be readily removed in the gas phase, leaving reactive unsaturated W—X (X = Br, OH) functional sites that are pivotal groups to trigger the catalytic activity of polynuclear systems such as tungsten polyoxometalates.[38] This latter point is reminiscent to that occurring in many organometallic reaction sequences in the condensed phase, being the metal—phosphane strength a useful parameter in the evaluation of possible reaction mechanisms, especially in catalysis.[39]

Herein, we present a comparative study on the gas-phase dissociation of bromine and hydroxo-containing cluster complexes of general formula $[W_3S_4(dmpe)_3(X)_3]^+$ (X = Br **1**$^+$, OH **2**$^+$) using ESI tandem mass spectrometry. Each of these **1**$^+$ and **2**$^+$ cation precursors provides access to product ions with the robust trinuclear W_3S_4 cluster unit that possess W—Br, W═O, and W—OH functional groups either on saturated or unsaturated metal sites. Complementary ion/molecule reactions with methanol as model substrate in conjunction with DFT calculations are also carried out to unravel the fundamental reactivity of these functional groups and determine which is the molecular basis responsible of the methanol activation.

2. Experimental Section

2.1. General Procedures. Compounds $[W_3S_4(dmpe)_3(Br)_3]PF_6$ ([**1**]PF_6)[40] and $[W_3S_4(dmpe)_3(OH)_3]PF_6$ ([**2**]PF_6)[35] were prepared according to literature procedures. Deuteration of the three hydroxo groups in cation **2**$^+$ is carried out by incubation of compound [**2**]PF_6 in CH_3CN:D_2O (1:1) mixtures for 5 min. The H/D exchange is quantitative and only involves the labile W—OH functional groups, as judged by the ESI mass spectrum where the isotopic pattern agrees perfectly with an increase of 3 Da with respect to the nondeuterated **2**$^+$ cluster cation. Acetonitrile (HPLC grade, 99.8%), methanol (HPLC grade, 99.8%), CD_3OD (99.8 atom % D), CH_3OD (99.8 atom % D), and $CH_3{}^{18}OH$ (95 atom % O) were obtained from Aldrich and used without further purification.

2.2. Mass Spectrometry. Electrospray ionization (ESI) and tandem mass experiments were conducted on a Quattro LC (quadrupole—hexapole—quadrupole) mass spectrometer with an orthogonal Z-spray-electrospray interface (Waters, Manchester, UK). Sample solutions were infused via syringe pump directly connected to the ESI source at a flow rate of 10 μL/min and a capillary voltage of 3.5 kV was used in the positive scan mode. The desolvation gas as well as nebulization gas was nitrogen at a flow of 7.5 and 1.3 L/min, respectively. ESI mass spectra of acetonitrile solutions of [**1**]PF_6 and [**2**]PF_6 recorded at low cone voltages (typically $U_c = 20-30$ V) promote the gas-phase formation of the pseudomolecular **1**$^+$ and **2**$^+$ cations. To investigate their characteristic gas-phase dissociation, we studied the collision-induced dissociation (CID) spectra of cations **1**$^+$ and **2**$^+$. For CID spectra, cations **1**$^+$ and **2**$^+$ (generated at low cone voltages) were mass-selected by using the first quadrupole (Q1) and interacted with argon in the hexapole collision cell under multiple-collision conditions (typically 7×10^{-4} mbar) at variable collision energies ($E_{laboratory} = 0-60$ eV) while scanning Q2 to monitor the ionic products of fragmentation. An isolation width of 1 Da was used in the first quadrupole analyzer. Aimed at confirming the fragmentation pathways proposed for the **1**$^+$ and **2**$^+$ cations, their fragmentation products **1a**$^+$, **2a**$^+$, and **2b**$^+$ (see below) were generated by "in source" fragmentation starting from **1**$^+$ and **2**$^+$ at different cone voltages (typically in the $U_c = 30-180$ range) and subsequently subjected to CID as described above.

The intrinsic ion—molecule reactivity of cations **1**$^+$ and **2**$^+$ and their fragmentation (**1a**$^+$, **1b**$^+$, **2a**$^+$, **2b**$^+$, and **2c**$^+$) products with methanol was also investigated. For ion—molecule reaction studies, the species of interest were gas-phase generated at different cone voltages (typically $U_c = 30$ V for the **1**$^+$ and **2**$^+$ cations whereas $U_c = 90$ V for the remaining species), mass-selected with Q1, and interacted with CH_3OH in the hexapole collision cell, while scanning Q2 to monitor the products of ion—molecule reactions. An isolation width of 1 Da was used in Q1 and the collision energy in the hexapole collision cell was nominally set to a value of $E_{laboratory} = 0$ eV to increase the residence time of the ions in the collision cell and to ensure that reactions take place at or near thermal energies. The neutral volatile substrates were introduced in the collision cell as a part of the collision gas at a pressure in the collision cell maintained at approximately 2×10^{-4} mbar. At these conditions, the primary ion beam is attenuated by ca. 20%, thus corresponding to single-collision conditions.[41] As previously reported,[42,43] tandem mass spectrometers with a QhQ configuration are not convenient for the determination of rate constants, and we refrain from reporting absolute values herein; however, the relative rates can be used to assess the trends in reactivity for the different mass-selected species. Relative reaction rates for each species were determined by correlating the reactivities to that of the most reactive ion investigated (in the present study **2b**$^+$). For this purpose, the amount of conversion of the mass-selected species was determined as $x_P = I_P/\sum I_i$, where I_P stands for the intensity of the mass-selected ion (that formally corresponds to the amount of nonreacted precursor ion) whereas the $\sum I_i$ term stands for the sum of intensities of all species in the ion—molecule spectra (that represent the initial amount of the precursor ion). The x_P term was then inserted into $kt = -\ln(x_P)$ (where k stands for the reaction rate of each precursor ion and t is the effective reaction time in the collision cell).[42,43] Due to the difficulties in having an accurate estimate about the effective length of the collision cell and thus the effective reaction time, relative reactions rates (k_{rel}) are reported as the ratio between the k value of a given species and that of the most reactive (**2b**$^+$) species. The experimentally observed relative rates were corrected for contributions from mere fragmentation, which occurred in some cases despite a collision energy nominally set to 0 eV. This implies that the contribution of these fragmentation peaks is taken into consideration in the $\sum I_i$ term of equation $x_P = I_P/\sum I_i$. The relative rates reported in Table 1 are averages of three independent measurements. Our experiments show that values obtained for k_{rel} varied less than 10% for the cationic cluster complexes studied.

TABLE 1: Relative Reaction Rates k_{rel} (%)[a] and Branching Ratios (%)[b] for the Condensation ($\Delta m = +14$) and Association ($\Delta m = +32$) Reaction of Mass-Selected Product Ions Generated from 1^+ and 2^+ with Methanol

mass-selected cation	k_{rel} (%)	$\Delta m = +14$	$\Delta m = +32$
$[W_3S_4(dmpe)_3(Br)_3]^+$ ($\mathbf{1}^+$)			
$[W_3S_4(dmpe)_2(Br)_3]^+$ ($\mathbf{1a}^+$)	16		100
$[W_3S_4(dmpe)(Br)_3]^+$ ($\mathbf{1b}^+$)	35		100
$[W_3S_4(dmpe)_3(OH)_3]^+$ ($\mathbf{2}^+$)			
$[W_3S_4(dmpe)_2(OH)_3]^+$ ($\mathbf{2a}^+$)	60	75	25
$[W_3S_4(dmpe)_2(OH)(O)]^+$ ($\mathbf{2b}^+$)	100	100	
$[W_3S_4(dmpe)(dmpe - H)(O)]^+$ ($\mathbf{2c}^+$)	22		100

[a] Reaction rates k_{rel} relative to cation $\mathbf{2b}^+$, which reacts with the highest rate (see the Experimental Section). [b] Branching ratios are defined as the relative intenisities of the products of ion molecule reactions corresponding to $\Delta m = 14$ (condensation) and $\Delta m = 32$ (association) normalized to $\Sigma = 100$.

2.3. DFT Calculations. The theoretical study used $[W_3S_4(PH_3)_6(OH)_3]^+$ as the molecular model for $[W_3S_4(dmpe)_3(OH)_3]^+$ ($\mathbf{2}^+$). This made attainable calculation times possible without changing the cluster coordination environment where phosphane and water elimination take place.[44] The calculations were conducted with the Becke hybrid density functional (B3LYP)[45] method as implemented in the Gaussian 03 program suite.[46] The double-ζ pseudo-orbital basis set LanL2DZ, in which W, S, O, and P atoms are represented by the relativistic core LanL2 potential of Los Alamos, was used.[47] Despite some shortcomings having been observed when applying the LanL2DZ basis set to other metal containing systems,[48] we have recently reported that the B3LYP/LanL2DZ proved to be a reliable tool for describing geometric, electronic structures and energetic profiles of M_3S_4 (M = Mo, W) cluster complexes isostructural to those studied in this work.[35,44,49] In the present case, deviations less that 5% were observed for the experimentally determined intermetallic distances in the $[W_3S_4(dmpe)_3(OH)_3]^+$ cation and the model complex, namely $[W_3S_4(PH_3)_6(OH)_3]^+$. The geometry optimizations were performed without any symmetry constraint followed by analytical frequency calculations to confirm that a minimum had been reached.

3. Results and Discussion

This work is organized as follows: a discussion of the gas-phase dissociation of cluster $\mathbf{1}^+$ and $\mathbf{2}^+$ cations upon CID conditions is followed by a description of the plausible fragmentation channels and product ion structures. For this purpose, isotope-labeling experiments in conjunction with theoretical calculation are employed. The section closes with the study of the bimolecular reactivity of the product ions formed with methanol aimed to elucidate the intrinsic reactivity of the W—Br and W—OH groups present in trinuclear W_3S_4 cluster cations.

3.1. Gas-Phase Dissociation of 1^+ and 2^+. The ESI-MS spectra of the trinuclear [**1**]PF_6 and [**2**]PF_6 complexes obtained under gentle conditions, which means a low cone voltage (U_c = 20−30 V), gave as base peak the expected pseudomolecular $[M]^+$ ions. The distinctive isotopic pattern displayed by these ions (mainly due to the presence of W) actually facilitates assignment of ion stoichiometry via comparison between experimental and theoretical isotopic patterns. However, the broad isotope pattern can also make small mass changes difficult to detect (e.g., losses of small fragments or during isotope labeling experiments). To circumvent this problem, the most prominent peak in the isotopomer pattern was mass selected and used to study their characteristic gas-phase dissociation. The CID spectra for the trinuclear $\mathbf{1}^+$ and $\mathbf{2}^+$ complexes are shown in Figure 1.

The gas-phase dissociation of $\mathbf{1}^+$ consists first of a loss of one diphosphane ligand to give the unsaturated $[W_3S_4(dmpe)_2(Br)_3]^+$ ($\mathbf{1a}^+$) (m/z 1219) at collision energies (CE) below $E_{laboratory}$ = 40 eV (eq 1). Gradually increasing the CE up to $E_{laboratory}$ = 60 eV enhances the fragmentation of a second diphosphane ligand for the $\mathbf{1}^+$ cation to yield $[W_3S_4(dmpe)Br_3]^+$ ($\mathbf{1b}^+$) (eq 2). The proposed fragmentation pathway for the $\mathbf{1}^+$ cation was further confirmed by investigating the CID spectra of $\mathbf{1a}^+$. Cation $\mathbf{1a}^+$ can be generated by "in-source" fragmentation (typically at U_c = 90V) and its CID spectra reveal the exclusive formation of the $\mathbf{1b}^+$ cation (see Figure S1 in the Supporting Information).

$$[W_3S_4(dmpe)_3(Br)_3]^+ (\mathbf{1}^+) \rightarrow [W_3S_4(dmpe)_2(Br)_3]^+ (\mathbf{1a}^+) + dmpe \quad (1)$$

$$[W_3S_4(dmpe)_2(Br)_3]^+ (\mathbf{1a}^+) \rightarrow [W_3S_4(dmpe)(Br)_3]^+ (\mathbf{1b}^+) + dmpe \quad (2)$$

The hydroxo-containing $\mathbf{2}^+$ cation first undergoes diphosphane evaporation at identical conditions to that observed for $\mathbf{1}^+$ (typically below $E_{laboratory}$ = 40 eV), followed by the evaporation of two water molecules at higher collision energies. The initial loss of one water molecule $[\mathbf{2} - H_2O]^+$ (m/z 1163) is also observed as a minor fragmentation channel at low collision energies. Remarkably, the loss of a second diphosphane ligand in $\mathbf{2}^+$ is suppressed in front of the most favorable evaporation of two water molecules. To obtain further insights on the origin of the two water evaporation processes, the gas-phase dissociation of the deuterated d^3-$\mathbf{2}^+$ homologue at the three hydroxo groups was also investigated. CID spectra of d^3-$\mathbf{2}^+$ reveal, besides the typical loss of one diphosphane ligand (eq 3), a first loss of D_2O (eq 4) ascribed to a deuterium migration between neighboring W—OD groups. With regard to the fragmentation channel involving a second water molecule, the experiments with d^3-$\mathbf{2}^+$ indicate that an additional terminal W—OD group and one hydrogen atom from the diphosphane ligand are involved (eq 5).

$$[W_3S_4(dmpe)_3(OD)_3]^+ (d^3\text{-}\mathbf{2}^+) \rightarrow [W_3S_4(dmpe)_2(OD)_3]^+ (d^3\text{-}\mathbf{2a}^+) + dmpe \quad (3)$$

$$[W_3S_4(dmpe)_2(OD)_3]^+ (d^3\text{-}\mathbf{2a}^+) \rightarrow [W_3S_4(dmpe)_2(OD)O]^+ (d^3\text{-}\mathbf{2b}^+) + D_2O \quad (4)$$

$$[W_3S_4(dmpe)_2(OD)O]^+ (d^3\text{-}\mathbf{2b}^+) \rightarrow [W_3S_4(dmpe)(dmpe\text{-}H)(O)]^+ (d^3\text{-}\mathbf{2c}^+) + HDO \quad (5)$$

The proposed fragmentation pathway for $\mathbf{2}^+$ cation was further confirmed by investigating the CID spectra of $\mathbf{2a}^+$ and $\mathbf{2b}^+$, which can be generated by "in-source" fragmentation (typically at U_c = 90V). The CID spectra of $\mathbf{2a}^+$ show the presence of the $\mathbf{2b}^+$ and $\mathbf{2c}^+$ cations while CID of $\mathbf{2b}^+$ reveal the exclusive formation of cation $\mathbf{2c}^+$ (see Figure S1 in the Supporting Information).

Hydrogen migration processes involving terminal O—H hydroxo or C—H diphosphane ligands are precedent in the gas-phase dissociation of transition metal complexes. On one hand, the gas-phase dissociation of the $[(cathecol)V(OH)_2]^+$ cation that

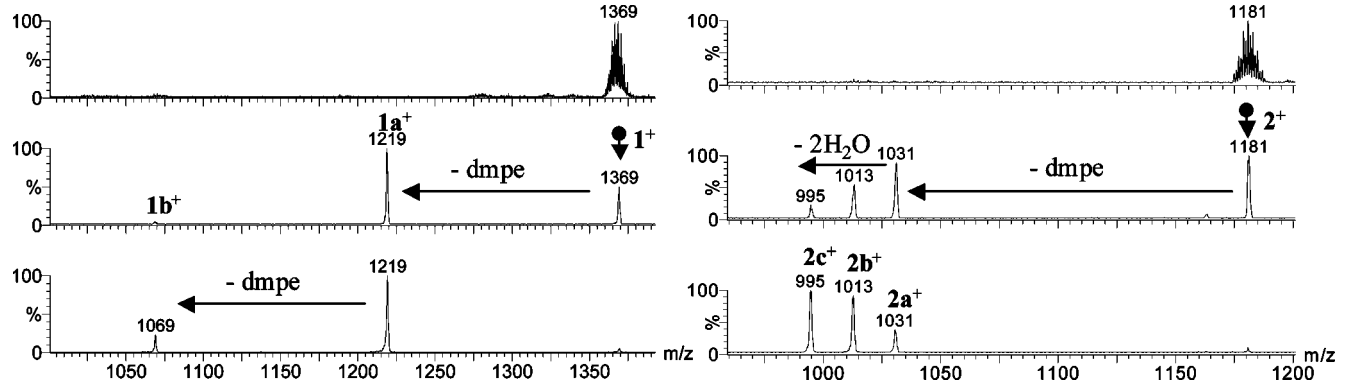

Figure 1. ESI mass spectrum (top) and product ion spectra at two collision energies, $E_{laboratory} = 40$ eV (middle) and $E_{laboratory} = 60$ eV (bottom) of mass-selected a) $[W_3S_4(dmpe)_3(Br)_3]^+$ ($\mathbf{1}^+$), and b) $[W_3S_4(dmpe)_3(OH)_3]^+$ ($\mathbf{2}^+$).

SCHEME 1

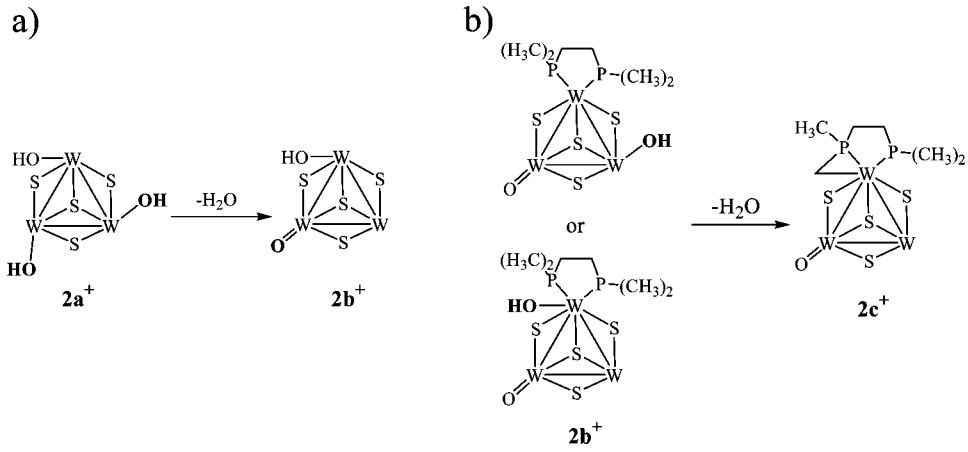

possesses two geminal hydroxo groups leads to the oxo $[V(cathecol)VO]^+$ product ion with concomitant water evaporation.[50] With regard to the formation of the $\mathbf{2b}^+$ cation according to eq 4, proton migration must occur between hydroxo groups that belong to different metal sites and consequently far from each other; for instance, bond distances involving the oxygen atoms from hydroxo group in cation $\mathbf{2}^+$ are ca. 5 Å according to X-ray diffraction experiments.[35] It is reasonable to hypothesize that the presence of sulfur-bridged ligands connecting these metal sites might facilitate such hydrogen transfer. A simplified drawing of the hydroxo groups involved is shown in Scheme 1.

On the other hand, hydrogen abstraction from the backbone of mono- and diphosphane ligands is ubiquitous in the gas-phase dissociation of palladium complexes.[51−53] For example, the gas-phase liberation of HBr is observed upon CID for the $[PdBr(P(Ph)_2(CH_2)_5P(Ph)_2)]^+$ cation and is proposed to occur through diphosphane backbone C—H activation to afford carbene-type product ions.[54] We hypothesize that the fragmentation channel that leads to the product ion $\mathbf{2c}^+$ (eq 5) switches the diphosphane ligand coordination mode from bidentate to carbene-type tridentate. Scheme 1b shows a simplified scheme of the plausible diphosphane coordination mode in the product ion $\mathbf{2c}^+$. This C—H activation mechanism would result in a much more strongly bounded diphosphane ligand and therefore can be invoked to account for the absence of a second diphosphane evaporation in cation $\mathbf{2}^+$. With the present experiments it is not possible to distinguish the diphosphane C—H group involved because of the presence of four nonequivalent methyl groups and four hydrogen atoms from the ethylene-bridged group. It must be stressed that no fragmentation of the W_3S_4 cluster core is detected at our experimental condition, revealing a high robustness of this trinuclear cluster unit. Before addressing the effects of the properties of the new gas-phase generated product ions (among them, ion composition as well as its coordination number) on their reactivity toward methanol, product ion structures are evaluated in the next section on the basis of DFT calculations.

3.2. DFT Studies on Plausible Product Ion Structures. Dissociation through the expulsion of neutral diphosphane ligands observed for $\mathbf{1}^+$ and $\mathbf{2}^+$ is ubiquitous in isostructural trinuclear molybdenum as well as cubane-type complexes, namely $[Mo_3S_4(dmpe)_3Cl_3]^+$ and $[Mo_3(M'CO)S_4(dmpe)_3Cl_3]^+$ ($M' =$ transition metal), respectively.[55,56] It is reasonable to assume that the first diphosphane liberation occurs through an equivalent mechanism for both $\mathbf{1}^+$ and $\mathbf{2}^+$, thus we have turned to DFT calculations to gain further insights on the product ion structures for the hydroxo $\mathbf{2a}^+$ cation as a case of study. We have used as a model system the trinuclear W_3S_4 cluster bearing two monophosphanes (PH_3) per tungsten site to optimize reaction intermediate structures at the B3LYP/LanL2DZ level. Optimized $\mathbf{2}^+$ and $\mathbf{2a}^+$ geometries and diphosphane dissociation energies are shown in Figure 2.

Removal of the first diphosphane ligand ($\mathbf{2}^+ \rightarrow \mathbf{2a}^+$) requires 21.5 kcal mol^{-1} and in general it is not associated to large variations in the main geometric features within the W_3S_4 cluster core. The unsaturated tungsten atom in $\mathbf{2a}^+$ presents shorter W—W distances (ca. 0.04 Å) than those involving saturated tungsten sites, thus resulting in a slight distortion of the W_3S_4 unit. The most significant geometric difference between $\mathbf{2}^+$ and $\mathbf{2a}^+$ has to do with the relative orientation of the terminal hydroxo group attached to the unsaturated metal site, which in

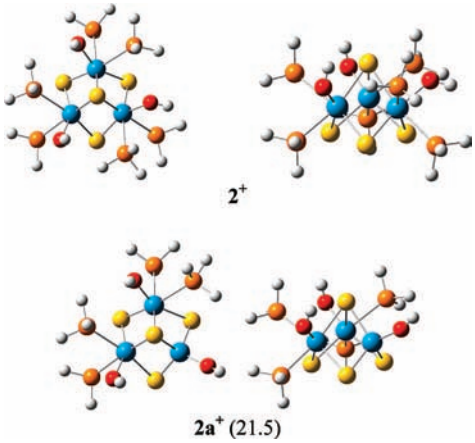

Figure 2. B3LYP optimized geometries (left, front view; right, side view) and diphosphane dissociation energies (kcal mol^{-1}).

2a$^+$ appears located trans to the μ_3-S capping sulfur atom leading to a pseudotetrahedral unsaturated tungsten site.

Because of the overall C_s symmetry for the **2a**$^+$ cation, the three hydroxo groups are not equivalent and, consequently, the water evaporation process that leads to cation **2b**$^+$ might operate through different proton migration processes. We have investigated three different proton migration processes: namely, (a) proton migration from the $W_{unsaturated}$—O*H* group (Scheme 2 a), (b) proton migration from one $W_{saturated}$—O*H* group to the $W_{unsaturated}$—O*H* group (Scheme 2b), and (c) proton migration between $W_{saturated}$—O*H* groups (Scheme 2c). Indeed, each of these proton migration processes can involve two different W—OH groups, thus resulting in a series of additional isomers (labeled as **2b′** in Figure 3). Figure 3 shows the calculated structure of the two isomeric forms (**2bn**$^+$ and **2bn′**$^+$; $n = 1, 2, 3$) for each intermediate.

According to the DFT calculations, two sets of isomers are energetically favored mainly determined by the identity of the ligand attached to the unsaturated tungsten site. Isomeric species possessing W═O (**2b1**$^+$ and **2b1′**$^+$) and W—OH (**2b3**$^+$ and **2b3′**$^+$) unsaturated groups are energetically favored in front of those lacking such groups, namely **2b2**$^+$ and **2b2′**$^+$. For example, the energetic difference between **2b3**$^+$ and **2b2′**$^+$ amounts ca. 20 kcal mol^{-1}. Given the close energetic stability between the **2bn**$^+$ and **2bn′**$^+$ ($n = 1, 2, 3$) pairs we will only refer to them as **2bn**$^+$ throughout the text. We have also considered the possibility that formation of W═O groups might produce decoordination of one arm of the diphosphane ligand. To simulate this process we have investigated the thermodynamics of the dissociation of one PH_3 in **2b2**$^+$ and **2b3**$^+$ cations (see the Supporting Information, Figure S2). Calculations show that decoordination of one PH_3 produces a slight destabilization of 3 kcal mol^{-1} for the **[2b2′-PH$_3$]**$^+$ and **[2b3′-PH$_3$]**$^+$ resulting species. Only the **[2b3-PH$_3$]**$^+$ cation is also slightly stabilized (2 kcal mol^{-1}) without breaking the W_3S_4 cuboidal unit.

Intermetallic distances of plausible **2b**$^+$ intermediates (see the Supporting Information) are all similar to that observed for the cluster **2**$^+$ and **2a**$^+$ precursors (ca. 2.77 Å), and only **2b1′**$^+$ shows a significantly longer W—W average distance (2.81 Å). Nevertheless, these values are still consistent with the presence of single W—W bonds. In addition, hydroxo orientations and W—OH interatomic distances also remain almost intact as compared with **2**$^+$ and **2a**$^+$. These results confirm our assumption that the trinuclear W_3S_4 cluster core is a very robust entity. The mechanism for the formation of the **2c**$^+$ cation, which contains a tridentate carbene-type diphosphane, from cation **2b**$^+$ is expected to be complex due to the large number of potential pathways. From one side, several isomeric forms for the **2b**$^+$ cation need to be considered, and on the other side, various hydrogen atoms (12 from CH_3 groups and 4 from CH_2 groups) can be a priori eliminated to produce the corresponding carbide. All this together has refrained us from undertaking this theoretical analysis.

3.3. Intrinsic Bimolecular Reactivity of W—X (X = Br, OH, and O) Functional Groups toward Methanol. Aimed to probe the intrinsic reactivity of the product ions formed upon CID conditions, we generate them by "in-source" fragmentation (typically at cone voltages in the $U_c = 90-180$ V range). The identity of the product ions generated either by CID or "in-source" fragmentation shares common features. The most significant difference is that "in-source" fragmentation spectra present additional product ions ascribed to the gas-phase adduct formation with adventious CH_3CN present in the cone region. Figure 4 shows the ESI mass spectra of cation **1**$^+$ recorded at $U_c = 90$ and 140 V to illustrate the "in-source" solvent adduct formation.

Besides the abundant presence of product ions **1a**$^+$ (*m*/*z* 1219) and **1b**$^+$ (*m*/*z* 1069), prominent peaks due to solvent adduct formation of the general formula [**1a**$^+$ + CH_3CN]$^+$ (*m*/*z* 1260) and [**1b**$^+$ + $n$$CH_3CN$]$^+$ ($n = 1, 2$) (*m*/*z* 1110 and 1151) are clearly observed. Additional minor peaks centered at *m*/*z* 1175 and 1129 are also observed. These species are neither observed upon CID of **1**$^+$ nor match the expected *m*/*z* values for additional adduct formation with CH_3CN molecules, therefore their origin has to be associated to minor impurities present in the starting [**1**](PF_6) material. According to their mass-to-charge ratio, these species are assigned to the mixed halide $[W_3S_4Br_2Cl(dmpe)_2]^+$ (*m*/*z* 1175) and $[W_3S_4BrCl_2(dmpe)_2]^+$ (*m*/*z* 1129) cations. This halide scrambling has incidentally been observed as a minor side reaction upon dissolving W_3S_4 complexes in chlorinated solvents used in its workup procedure.[40]

At identical cone voltages to that used for the **1**$^+$ cation, product ions resulting from the hydroxo-containing **2**$^+$ cation, namely **2a**$^+$, **2b**$^+$, and **2c**$^+$, also undergoes solvent adduct formation in the cone region. The results of the reactions between cations **1**$^+$, **2**$^+$, and their product ions with methanol are collected in Table 1.

In the reaction of mass-selected **1**$^+$ (*m*/*z* 1369) and **2**$^+$ (*m*/*z* 1181) cations with CH_3OH, no reaction products are observed in agreement with the absence of unsaturated tungsten sites. The unsaturated ionic fragments that result from diphosphane liberation were all found to undergo two different reaction paths depending on whether methanol is simply associated or condensated with the concomitant water formation. Hence, the reaction of the unsaturated **1a**$^+$ (*m*/*z* 1119) and **1b**$^+$ (*m*/*z* 1069) cations with CH_3OH exclusively produces molecular association ($\Delta m = +32$) to afford the adducts [**1a** + CH_3OH]$^+$ (*m*/*z* 1151) and [**1a** + CH_3OH]$^+$ (*m*/*z* 1101), respectively. Neither for **1a**$^+$ nor for **1b**$^+$ cations is there evidence of methanol cleavage in the gas phase.

In the case of mass-selected **2c**$^+$ cation (*m*/*z* 995) containing a tridentate carbene-type diphosphane, an association adduct with CH_3OH ($\Delta m = +32$) is observed consistent with the absence of terminal hydroxo groups in structure **2c**$^+$. An increase in the relative rate of adduct formation for **1b**$^+$ with respect to that of mass-selected **1a**$^+$ and **2c**$^+$ ions (see Table 1) gives support to the presence of additional vacant sites in **1b**$^+$. That is, the presence of up to four vacant coordination sites in **1b**$^+$ cation in front of the two positions available in **1a**$^+$ and **2c**$^+$ statistically favors coordination of neutral reagents.

SCHEME 2

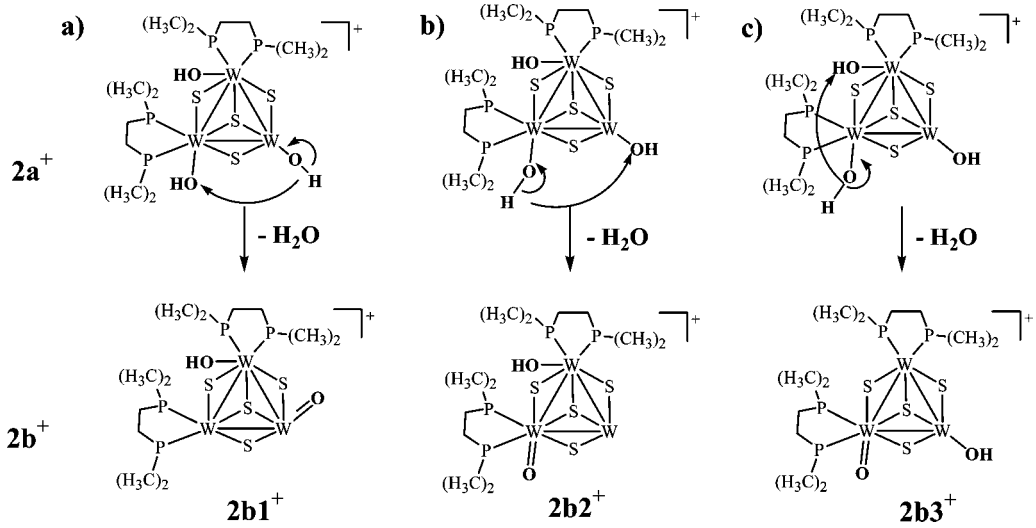

The $\mathbf{2a}^+$ cation (m/z 1031) was generated from $\mathbf{2}^+$ by adjusting the cone voltage to $U_c = 90$ V. Figure 5a shows the spectra for the reaction of CH_3OH (top), CD_3OD (middle), and $CH_3{}^{18}OH$ (bottom) with mass-selected $\mathbf{2a}^+$.

The reaction with CH_3OH of the unsaturated $\mathbf{2a}^+$ cation reveals besides formal addition of CH_3OH condensation reactions concomitant with the loss of H_2O ($\Delta m = +32 - 18 = +14$) and the formation of terminal methoxo functional groups (eq 6). To evaluate the plausible presence of other hidden reactions due to isobaric overlapping and the intimate mechanistic picture (O—H or C—O methanol cleavage) for the condensation step, isotopic labeling studies were also performed for CD_3OD and $CH_3{}^{18}OH$ reacting with cation $\mathbf{2a}^+$. These results are consistent with binding of methoxo ligand from methanol and elimination of hydroxo ligand as neutral water (see eqs 7 and 8). An homologous methanol cleavage mechanism has been observed for the reaction with $[CpZr{-}OH]^+$ for which a "four-center-four-electron" transition state has been proposed.[57]

$$[W_3S_4(dmpe)_3(OD)_3]^+ (\mathbf{2a}^+) \rightarrow [W_3S_4(dmpe)_2(OH_2)(OCH)_3]^+ + H_2O \quad (6)$$

$$[W_3S_4(dmpe)_3(OD)_3]^+ (\mathbf{2a}^+) + CD_3OD \rightarrow [W_3S_4(dmpe)_2(OH)_2(OCD_3)]^+ + HDO \quad (7)$$

$$[W_3S_4(dmpe)_3(OD)_3]^+ (\mathbf{2a}^+) + CH_3{}^{18}OH \rightarrow [W_3S_4(dmpe)_2(OH)_2(^{18}OCH_3)]^+ + H_2O \quad (8)$$

The characteristic bimolecular reactivity for the $\mathbf{2a}^+$ cation with methanol can be regarded as direct evidence of the presence of unsaturated W—OH functional groups and can be subsequently used to corroborate the presence of such groups in the closely related $\mathbf{2b}^+$ cation. Theoretical calculations suggest that $\mathbf{2b1}^+$ and $\mathbf{2b3}^+$ isomers possessing unsaturated W—OH and W═O functional groups, respectively (see Figure 3), are very close in energy and that these two species are energetically favored in front of the $\mathbf{2b2}^+$ cation. Therefore, ion−molecule reactions toward methanol may provide crucial input for structural determinations. We also consider the possibility that $\mathbf{2b}^+$ ions generated in the ESI source may possess different structures, not only due to isobaric interferences but also as a consequence of collisional-induced rearrangements occurring

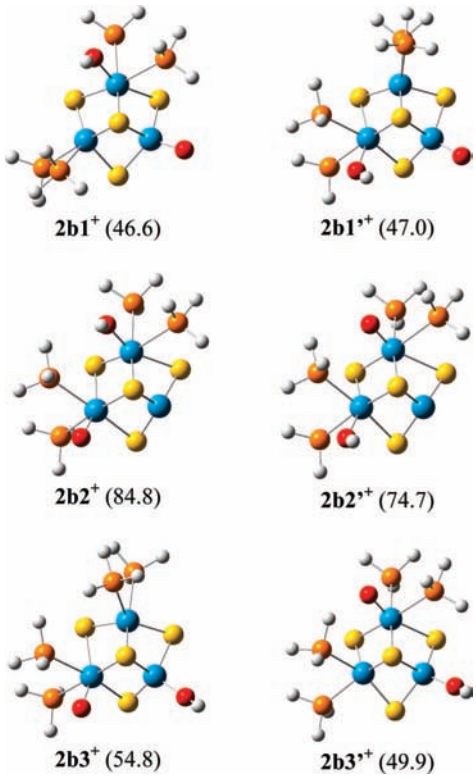

Figure 3. B3LYP optimized geometries and H_2O dissociation energies (kcal mol^{-1}).

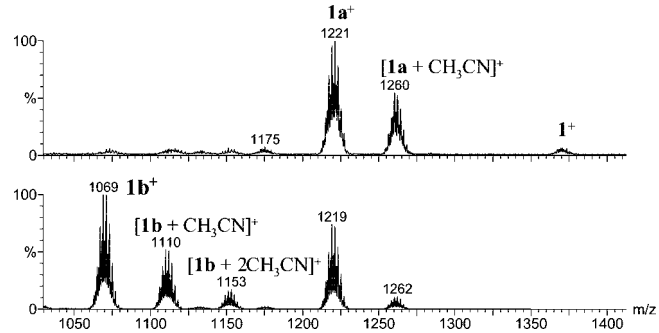

Figure 4. ESI mass spectra of compound $[\mathbf{1}]PF_6$ dissolved in acetonitrile at cone voltages $U_c = 90$ (top) and 140 V (bottom).

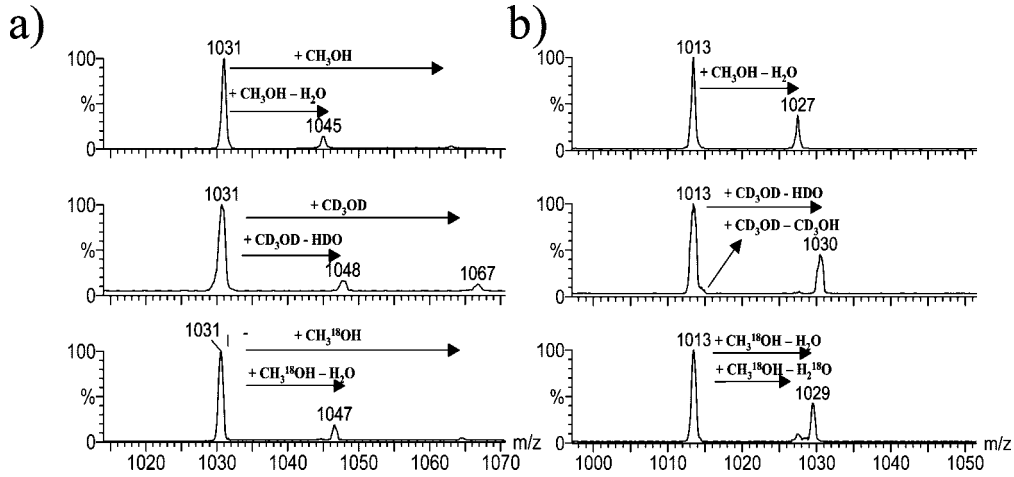

Figure 5. Mass spectra showing the reaction of CH_3OH (top), CD_3OD (middle), and $CH_3{}^{18}OH$ (bottom) with mass-selected (a) $\mathbf{2a}^+$ and (b) $\mathbf{2b}^+$.

in the source region. Thus, it is reasonable to hypothesize that a mixture of $\mathbf{2b1}^+/\mathbf{2b3}^+$ and $\mathbf{2b2}^+$ cations might be formed in the ESI process provided that both sets of isomers are separated by a reasonable barrier (typically 20 kcal/mol). Specifically, if a mixture of isomeric ions is formed upon ionization, their ratio is likely to depend on the ionization conditions and this latter can be tuned by modifying the cone voltage, i e., the amount of collisional activation to the formed cations. Hence, ion−molecule reactions were carried out on product $\mathbf{2b}^+$ (*m*/*z* 1013) cations generated at different cone voltages (in the $U_c = 90-180$ V range) in order to allow for a deconvolution of the reactivities of $\mathbf{2b1}^+$, $\mathbf{2b2}^+$, and $\mathbf{2b3}^+$.

The primary product ions upon reaction of $\mathbf{2b}^+$ (*m*/*z* 1013) (generated at $U_c = 90$ V where the presence of isomeric $\mathbf{2b1}^+$ and $\mathbf{2b3}^+$ cations is expected to be dominant) with CH_3OH correspond to the sole condensation of CH_3OH (eq 9) concomitant with the loss of H_2O ($\Delta m = +32 - 18 = +14$) (see Figure 5b). On the basis of the previously observed reactivity for the $\mathbf{2a}^+$ cation, the bimolecular reactivity of $\mathbf{2b}^+$ is consistent with the presence of (at least) one isomer with one terminal unsaturated W−OH group and therefore corroborates that product ion $\mathbf{2b3}^+$ is a prominent isomer present in the mass selected $\mathbf{2b}^+$ (at *m*/*z* 1013) ion beam. Further insights are gained from the reaction of $\mathbf{2b}^+$ with CD_3OD or ^{18}O-enriched methanol.

$$[W_3S_4(dmpe)_2(OH)O]^+ (\mathbf{2b}^+) + CH_3OH \rightarrow [W_3S_4(dmpe)_2(OCH_3)O]^+ + H_2O \quad (9)$$

$$[W_3S_4(dmpe)_2(OH)O]^+ (\mathbf{2b}^+) + CD_3OD \rightarrow [W_3S_4(dmpe)_2(OCD_3)O]^+ + HDO \quad (10)$$

$$[W_3S_4(dmpe)_2(OH)O]^+ (\mathbf{2b}^+) + CH_3{}^{18}OH \rightarrow [W_3S_4(dmpe)_2(^{18}OCH_3)O]^+ + H_2O \quad (11)$$

$$[W_3S_4(dmpe)_2(OH)O]^+ (\mathbf{2b}^+) + CH_3{}^{18}OH \rightarrow [W_3S_4(dmpe)_2(OCH_3)O]^+ + H_2{}^{18}O \quad (12)$$

Upon reaction of $\mathbf{2b}^+$ cation with CD_3OD, besides the formal condensation reaction according to eq 10, an additional bimolecular reaction is observed that consists of the partial H/D scrambling. The use of CH_3OD supports that this H/D scrambling comes from the alcohol deuterium atom. The reaction of mass-selected $\mathbf{2b}^+$ with $CH_3{}^{18}OH$ proceeds according to eqs 11 and 12, where binding of methoxo ligand from methanol and elimination of hydroxo ligand as neutral water competes with the releasing of $H_2{}^{18}O$ as a result of methanol C−O activation. These labeling experiments are also consistent with the lack of reactivity of the W=O (present in isomer $\mathbf{2b1}^+$) groups toward methanol. Identical bimolecular reactivity toward alcohols has been reported for the hydroxo $[W_2O_6(OH)]^-$ anion, which possesses both terminal hydroxo and oxo groups.[31]

Aimed at gaining further insights on the methanol condensation step observed for $\mathbf{2a}^+$ and $\mathbf{2b}^+$, we have undertaken a theoretical study of the energy profile for this reaction channel. As mentioned above, ion−molecule reaction and DFT results point toward the $\mathbf{2b3'}^+$ cation as thre dominant isomer in the mass-selected $\mathbf{2b}^+$ ion beam, and therefore the computational study was restricted to this cation. The calculated potential energy profiles and the optimized geometries for all stationary points for the reaction between the $\mathbf{2a}^+$ cation and methanol are presented in Figure 6. A similar mechanistic picture is also applicable to the $\mathbf{2b3'}^+$ (see the Supporting Information, Figure S3).

The initial step for the reaction between $\mathbf{2a}^+$ and methanol is the formation of the $[\mathbf{2a}\cdots CH_3OH]^+$ complex, which is bound by 28.9 kcal/mol below the entrance $\mathbf{2a}^+ + CH_3OH$ channel. In a following alcohol condensation step, a CH_3O-H bond cleavage occurs to give the $[\mathbf{2d}\cdots H_2O]^+$ isomer, which is 8.6 kcal mol^{-1} more unstable than the previous intermediate. This step proceeds via the transition state $\mathbf{TS_{2a\text{-}2d}}$ with an energy barrier of ca. 13.3 kcal mol^{-1}. The CH_3OH and OH arrangement around the unsaturated tungsten site in $TS_{\mathbf{2a\text{-}2d}}$ define a four-membered ring that closely resembles the "four-center-four-electron" transition state proposed for the methane activation by M_3O_9 group 6 oxides.[58] At this point, the water molecule in $[\mathbf{2d}\cdots H_2O]^+$ readily dissociates to give the reaction products, namely $\mathbf{2d}^+$ and H_2O. Hence, the energetically favored formation of the $[\mathbf{2a}\cdots CH_3OH]^+$ complex can be considered as the driving force of the reaction to give the condensation products in an overall exothermic process (−3.6 kcal mol^{-1}). Remarkably, this mechanistic picture agrees with our experimental observation where the methoxo ligand from methanol coordinates to the metal and the hydroxo group is eliminated as neutral water (see eqs 7 and 8).

Despite both $\mathbf{2a}^+$ and $\mathbf{2b}^+$ cations having identical molecular size (and consequently identical residence time in the collision cell) and equivalent W−OH reactive groups and being isoelec-

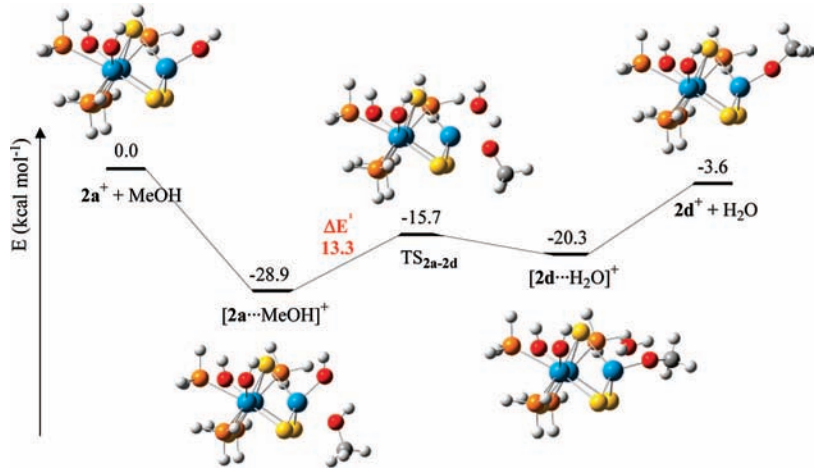

Figure 6. Potential energy profile of the reaction $[W_3S_4(PH_3)(OH)_3]^+$ (**2a**)$^+$ + $CH_3OH \rightarrow [W_3S_4(PH_3)_4(OH)_2(OCH_3)]^+$ (**2d**$^+$) + H_2O. Energies are given in kcal mol^{-1}.

tronic, the relative rate of methanol condensation for the **2b**$^+$ cation is significantly faster than that of **2a**$^+$. This experimental evidence is remarkable since the gas-phase generation of **2b**$^+$ may indeed result in a mixture of **2b1**$^+$ and **2b3**$^+$ isomers for which only **2b3**$^+$ is expected to contribute to the methanol condensation pathway. However, it cannot be definitively ruled out that the ion−molecule reactions may themselves also induce structural rearrangements;[59,60] in particular **2b1**$^+$ to **2b3**$^+$ isomerization may occur upon reaction with CH_3OH as this step essentially corresponds to a proton migration process. Steric considerations are also likely responsible of the differences found in the methanol condensation rates. As can be inferred from Figures 3 and 4 (see above), the orientation of the unsaturated W−OH groups in cations **2a**$^+$ and **2b3**$^+$ is quite similar. However, for cation **2a**$^+$, the diphosphane ligands on the neighboring tungsten sites cause the W−OH reaction site to be sterically hindered. For the **2b3**$^+$ cation that results from water elimination from **2a**$^+$, the unsaturated W−OH group is surrounded by partially unsaturated neighboring tungsten sites where the diphosphane ligands are rearranged as a consequence of the water elimination, thus leaving less hindered unsaturated W−OH sites.

We also investigate the effect of increasing the internal energy deposited on the **2b**$^+$ cation (i.e., sampling at high cone voltages) on its ion−molecule reaction with methanol. These results indicate a decrease in the methanol condensation channel relative to the adduct methanol formation and for example at $U_c = 180$ V, methanol adduct formation is dominant (see Figure 7).

This experimental observation can be ascribed to the presence of the **2b2**$^+$ cation formed at high cone voltages either via direct fragmentation from **2a**$^+$ or via isomerization of the **2b1**$^+$ and **2b3**$^+$ cations. In this sense, isomerization of **2b1**$^+$ and **2b3**$^+$ to yield **2b2**$^+$ formally corresponds to the migration of a diphosphane ligand between tungsten sites. Such migration processes involving phosphanes are precedent in the gas-phase ion chemistry of gold complexes.[61]

4. Conclusions

A combination of various experimental tandem mass experiments allows a rather comprehensive description of the product ions involved in the successive fragmentation of trinuclear sulfides $[W_3S_4(dmpe)_3(Br)_3]^+$ (**1**$^+$) and $[W_3S_4(dmpe)_3(OH)_3]^+$ (**2**$^+$) bearing diphosphanes and terminal W−X (Br and OH) functional groups. The presence of these latter functional groups heavily determines the preferred gas-phase dissociation. Deu-

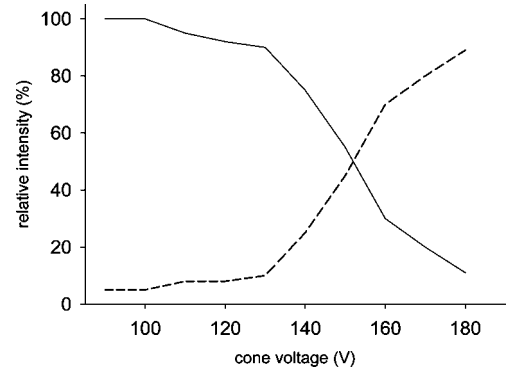

Figure 7. Normalized fractions of adduct formation (---) and condensation (−) upon reaction of mass-selected **2b**$^+$ ions (*m*/*z* 1012) with CH_3OH, generated upon ESI at variable cone voltages.

terium labeling experiments in conjunctions with DFT calculations at the B3LYP/LanL2DZ level are used to evaluate plausible product ions structures. These results indicate that upon gas-phase dissociation, each of these **1**$^+$ and **2**$^+$ precursor cations generate an assortment of product ions having all of them a robust trinuclear W_3S_4 cluster unit that possess W−Br, W=O, and W−OH functional groups either on saturated or unsaturated metal sites. Ion/molecule reactions with CH_3OH, CD_3OD, and $CH_3{}^{18}OH$ are investigated in order to corroborate product ion structures and to unravel the fundamental reactivity of these functional groups aimed at determining the molecular basis responsible for the plausible W_3S_4-based methanol activation. Our results show that ion−molecule reactions of W_3S_4 cations are strongly affected by the identity of the terminal W−X (X = Br, OH) functional groups as well as the coordinative saturation at the metal sites. In particular, the removal of one diphosphane ligand upon CID conditions is common to **1**$^+$ and **2**$^+$ cations and is critical to generate reactive metal sites. This gas-phase behavior is reminiscent of that generally observed in the condensed phase for metal phosphane complexes in which M−P decoordination−coordination is critical to trigger substrate activation at the metal center.

In the present study, only unsaturated W−OH groups produce methanol condensation at near thermal conditions to afford methoxo W−OCH_3 groups whereas the W−Br proved to be inert. According to labeling experiments and DFT calculations for those species bearing terminal W−OH groups, gas-phase methanol cleavage occurs through a "four-electron-four-center" mechanism analogous to that reported for the methane

activation mediated by group 6 (M_3O_9; M = Cr, Mo, W) metal oxides.[58] Preliminary results show that W_3S_4 cations bearing methoxo groups can also be generated in the source region by ESI of methanol solutions of the hydroxo $\mathbf{2}^+$ cation, which can be subsequently subjected to collision-induced dissociation to generate formaldehyde. These results prompt us to further investigate the reactivity of different alcohols as well as other M_3Q_4 (M = Mo, W; Q = S, Se) cluster units to obtain deeper insights on the potential of trinuclear group VI complexes as a model for the alcohol to aldehyde transformation. In this context, further theoretical work will be done using other combinations of pseudopotentials and basis sets aimed at comparing the results with those obtained in the present work. The information gained here extends the knowledge already gathered around the group 6 metal oxide reactivities, in particular it complements the fundamental characteristics of the dinuclear homo- and heteronuclear $[M_2O_6(OH)]^-$ (M = Mo, W) anions,[20,24,31,33] or those of the closely related trinuclear $[W_3O_9]^-$ anions, also with a triangular arrangement of tungsten atoms.[10,19,62]

Acknowledgment. This work was supported by the Spanish Ministerio de Educación y Ciencia (MEC) and EU FEDER (Project CTQ2005-09270-C02-01), and Fundació Bancaixa-Universitat Jaume I (Grant P1.1B2007-12). The authors also are grateful to the Servei d'Informatica and the Serveis Centrals d'Instrumentació Científica (SCIC) of the Universitat Jaume I for providing us with computing time and spectrometric facilities.

Supporting Information Available: Complete reference for Gaussian 03 and product ion spectra for the $\mathbf{1a}^+$, $\mathbf{2a}^+$, and $\mathbf{2b}^+$ (Figure S1) cations mentioned in the text; DFT-computed Cartesian coordinates and their electronic E and global reaction E_r energies for species relevant to each of the fragmentation pathways (Figure S2) described in the text; and energetic profile (Figure S3) and DFT-computed Cartesian coordinates and optimized electronic energies for the reaction of methanol with the $\mathbf{2b3}'^+$ cation. This material is available free of charge via the Internet at http://pubs.acs.org.

References and Notes

(1) Gazzoli, D.; Valigi, M.; Dragone, R.; Marucci, A.; Mattei, G. *J. Phys. Chem. B* **1997**, *101*, 11129.
(2) Bigey, C.; Hilaire, L.; Maire, G. *J. Catal.* **2001**, *198*, 208.
(3) Ji, S. F.; Xiao, T. C.; Li, S. B.; Xu, C. Z.; Hou, R. L.; Coleman, K.; Green, M. L. H. *Appl. Catal., A* **2002**, *225*, 271.
(4) Mamede, A. S.; Payen, E.; Grange, P.; Poncelet, G.; Ion, A.; Alifanti, M.; Parvulescu, V. I. *J. Catal.* **2004**, *223*, 1.
(5) Ono, Y. *Catal. Today* **2003**, *81*, 3.
(6) Jibril, B. Y.; Elbashir, N. O.; Al-Zahrani, S. M.; Abasaeed, A. E. *Chem. Eng. Process.* **2005**, *44*, 835.
(7) Kocon, M.; Michorczyk, P.; Ogonowski, J. *Catal. Lett.* **2005**, *101*, 53.
(8) Yoshinaga, Y.; Kudo, M.; Hasegawa, S.; Okuhara, T. *Appl. Surf. Sci.* **1997**, *121*, 339.
(9) Wang, Y. D.; Chen, Q. L.; Yang, W. M.; Xie, Z. K.; Xu, X.; Huang, D. *Appl. Catal., A* **2003**, *250*, 25.
(10) Kim, Y. K.; Rousseau, R.; Kay, B. D.; White, J. M.; Dohnálek, Z. *J. Am. Chem. Soc.* **2008**, *130*, 5059.
(11) Soares, A. P. V.; Portela, M. F. *Catal. Rev. Sci. Eng.* **2005**, *47*, 125.
(12) Parent, D. C.; Anderson, S. L. *Chem. Rev.* **1992**, *92*, 1541.
(13) Ervin, K. M. *Int. Rev. Phys. Chem.* **2001**, *20*, 127.
(14) Zemski, K. A.; Justes, D. R.; Castleman, A. W., Jr. *J. Phys. Chem. B* **2002**, *106*, 6136.
(15) Armentrout, P. B. *Eur. J. Mass Spectrom.* **2003**, *9*, 531.
(16) O'Hair, R. A. J.; Khairallah, G. N. *J. Clust. Sci.* **2004**, *15*, 331.
(17) O'Hair, R. A. J. *Chem. Commun.* **2006**, 1469.
(18) Fu, G.; Xu, X.; Lu, X.; Wan, H. L. *J. Am. Chem. Soc.* **2005**, *127*, 3989.
(19) Sun, Q.; Rao, B. K.; Jena, P.; Stolcic, D.; Kim, Y. D.; Gantefor, G.; Castleman, A. W., Jr. *J. Chem. Phys.* **2004**, *121*, 9417.
(20) Zhai, H. J.; Huang, X.; Cui, L. F.; Li, X.; Li, J.; Wang, L. S. *J. Phys. Chem. A* **2005**, *109*, 6019.
(21) Zhai, H. J.; Huang, X.; Waters, T.; Wang, X. B.; O'Hair, R. A. J.; Wedd, A. G.; Wang, L. S. *J. Phys. Chem. A* **2005**, *109*, 10512.
(22) Li, S.; Dixon, D. A. *J. Phys. Chem. A* **2006**, *110*, 6231.
(23) Huang, X.; Zhai, H. J.; Li, J.; Wang, L. S. *J. Phys. Chem. A* **2006**, *110*, 85.
(24) Huang, X.; Zhai, H. J.; Waters, T.; Li, J.; Wang, L. S. *Angew. Chem., Int. Ed.* **2006**, *45*, 657.
(25) Li, S.; Dixon, D. A. *J. Phys. Chem. A* **2007**, *111*, 11093.
(26) Lau, T. C.; Wang, J.; Guevremont, R.; Siu, K. W. M. *J. Chem. Soc., Chem. Commun.* **1995**, 877.
(27) Deery, M. J.; Howarth, O. W.; Jennings, K. R. *J. Chem. Soc., Dalton Trans.* **1997**, 4783.
(28) Walanda, D. K.; Burns, R. C.; Lawrance, G. A.; Nagy-Felsobuki, E. I. *J. Chem. Soc., Dalton Trans.* **1999**, 311.
(29) Feyel, S.; Waters, T.; O'Hair, R. A. J.; Wedd, A. G. *Dalton Trans.* **2004**, 4010.
(30) Waters, T.; Wang, X. B.; Li, S.; Kiran, B.; Dixon, D. A.; Wang, L. S. *J. Phys. Chem. A* **2005**, *109*, 11771.
(31) Waters, T.; O'Hair, R. A. J.; Wedd, A. G. *J. Am. Chem. Soc.* **2003**, *125*, 3384.
(32) Yang, X.; Waters, T.; Wang, X. B.; O'Hair, R. A. J.; Wedd, A. G.; Li, J.; Dixon, D. A.; Wang, L. S. *J. Phys. Chem. A* **2004**, *108*, 10089.
(33) Waters, T.; O'Hair, R. A. J.; Wedd, A. G. *Inorg. Chem.* **2005**, *44*, 3356.
(34) Gilje, J. W.; Roesky, H. W. *Chem. Rev.* **1994**, *94*, 895.
(35) Basallote, M. G.; Feliz, M.; Fernández-Trujillo, M. J.; Llusar, R.; Safont, V. S.; Uriel, S. *Chem. Eur. J.* **2004**, *10*, 1463.
(36) Basallote, M. G.; Estevan, F.; Feliz, M.; Fernández-Trujillo, M. J.; Hoyos, D. A.; Llusar, R.; Uriel, S.; Vicent, C. *Dalton Trans.* **2004**, 530.
(37) Llusar, R.; Uriel, S. *Eur. J. Inorg. Chem.* **2003**, 1271.
(38) Kamata, K.; Kotani, M.; Yamaguchi, K.; Hikichi, S.; Mizuno, N. *Chem. Eur. J.* **2007**, *13*, 639.
(39) Westmore, J. B.; Rosenberg, L.; Hooper, T.; Willet, G. D.; Fisher, K. J. *Organometallics* **2002**, *21*, 5688.
(40) Estevan, F.; Feliz, M.; Llusar, R.; Mata, J. A.; Uriel, S. *Polyhedron* **2001**, *20*, 527.
(41) Holmes, J. L. *Org. Mass Spectrom.* **1985**, *20*, 169.
(42) Schröder, D.; Holthausen, M. C.; Schwarz, H. *J. Phys. Chem. B* **2004**, *108*, 14407.
(43) Trage, C.; Diefenbach, M.; Schröder, D.; Schwarz, H. *Chem. Eur. J.* **2006**, *12*, 2454.
(44) Feliz, M.; Llusar, R.; Andres, J.; Berski, S.; Silvi, B. *New J. Chem.* **2002**, *26*, 844.
(45) Lee, C. T.; Yang, W. T.; Parr, R. G. *Phys. Rev. B.* **1988**, *37*, 785.
(46) Pople, J. A.; et al. *Gaussian03*; Gaussian Inc.: Pittsburgh, PA, 2003.
(47) Hay, J.; Wadt, R. *J. Chem. Phys.* **1985**, *82*, 270.
(48) de Jongh, G. T.; Solà, M.; Visscher, L.; Bickelhaupt, F. M. *J. Chem. Phys.* **2004**, *121*, 9982.
(49) Algarra, A. G.; Basallote, M G.; Feliz, M.; Fernández-Trujillo, M. J.; Llusar, R.; Safont, V. S. *Chem. Eur. J.* **2006**, *12*, 1413.
(50) Kaczorowska, M.; Schröder, D.; Schwarz, H. *Eur. J. Inorg. Chem.* **2005**, 2919.
(51) Henderson, W.; Fawcett, J.; Kemmit, R. D. W.; McKenna, P.; Russell, D. R. *Polyhedron* **1997**, *16*, 2455.
(52) McCaffery, L. J.; Henderson, W.; Nicholson, B. K.; Mackay, J. E.; Dinger, M. B. *J. Chem. Soc., Dalton Trans.* **1997**, 2577.
(53) Qian, R.; Guo, H.; Liao, Y.; Wang, H.; Zhang, X.; Guo, Y. *Rapid Commun. Mass Spectrom.* **2006**, *20*, 589.
(54) Neo, K. E.; Neo, Y. C.; Chien, S. W.; Tan, G. K.; Wilkins, A. L.; Henderson, W.; Hor, T. S. A. *Dalton Trans.* **2004**, 2281.
(55) Algarra, A. G.; Basallote, M. G.; Castillo, C. E.; Corao, C.; Llusar, R.; Fernández-Trujillo, M. J.; Vicent, C. *Dalton Trans.* **2006**, 5725.
(56) Guillamon, E.; Llusar, R.; Pozo, O.; Vicent, C. *Int. J. Mass Spectrom.* **2006**, *254*, 28.
(57) Richardson, D. E.; Lang, G. H. L.; Crestoni, E.; Ryan, M. F.; Eyler, J. R. *Int. J. Mass Spectrom.* **2001**, *204*, 255.
(58) Fu, G.; Xu, X.; Wan, H. *Catal. Today* **2006**, *117*, 133.
(59) Becker, H.; Schröder, D.; Zummack, W.; Schwarz, H. *J. Am. Chem. Soc.* **1994**, *116*, 1096.
(60) Beyer, M. K.; Berg, C. B.; Achatz, U.; Joos, S.; Niedner-Schatteburg, G.; Bondybey, V. E. *Mol. Phys.* **2001**, *99*, 699.
(61) Khairallah, G. N.; O'Hair, R. A. J.; Bruce, M. I. *Dalton Trans.* **2006**, 3699.
(62) Bondarchuk, O.; Huang, X.; Kim, J.; Kay, B. D.; Wang, L. S.; White, J. M.; Dohnálek, Z. *Angew. Chem., Int. Ed.* **2006**, *45*, 4786.

JP804263Q